Electronic Supplementary Information

The effect of substituents and molecular aggregation on the room temperature phosphorescence of a twisted π-system

Cristian A. M. Salla,[1] Giliandro Farias,[2] Ludmilla Sturm,[3] Pierre Dechambenoit,[3] Fabien Durola,[3] Murat Aydemir,[4,5] Bernardo de Souza,[2*] Harald Bock,[3*] Andrew P. Monkman,[4*] Ivan H. Bechtold[1*]

*Corresponding authors: bernadsz@gmail.com; harald.bock@crpp.cnrs.fr; ap.monkman@durham.ac.uk; ivan.bechtold@ufsc.br.

[1]Department of Physics, Universidade Federal de Santa Catarina, 88040-900 Florianópolis, SC, Brazil

[2]Department of Chemistry, Universidade Federal de Santa Catarina, 88040-900 Florianópolis, SC, Brazil

[3]Centre de Recherche Paul Pascal, CNRS & Université de Bordeaux, 115, av. Schweitzer, 33600 Pessac, France

[4]Department of Physics, Durham University, South Road, Durham, DH1 3LE, U.K.

[5]Erzurum Technical University, Department of Fundamental Sciences, Erzurum, Turkey

Table of Contents

1. Results and discussion

1.1 Single crystal x-ray diffraction

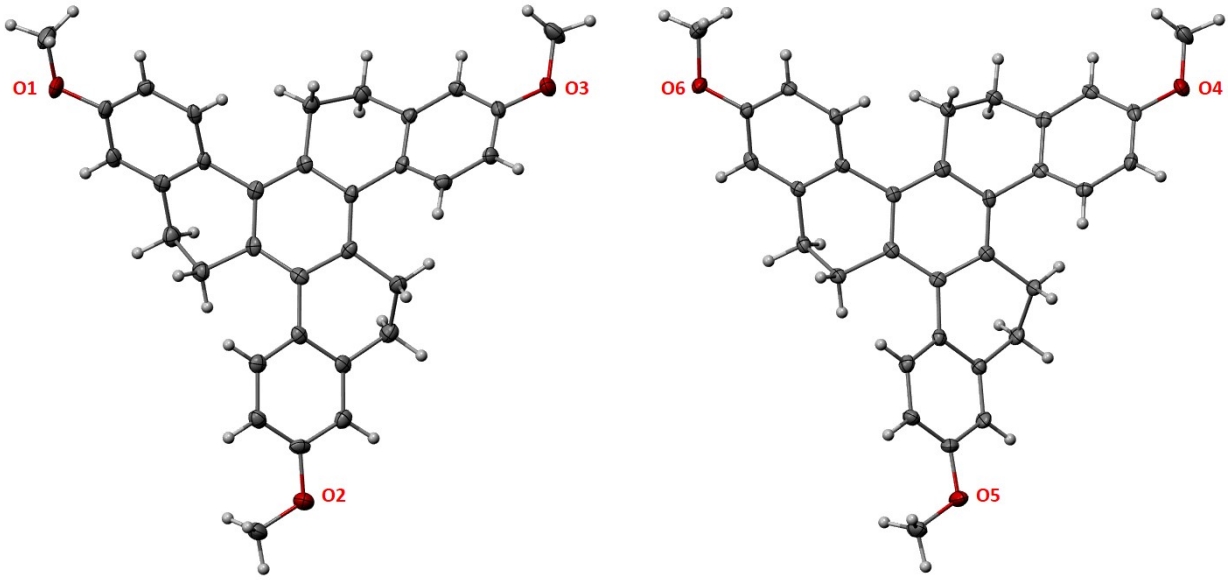

Figure S1. ORTEP plot of the molecular structure. ORTEP-type view of the two crystallographically different molecules of **HTX-MeO** at 120 K with thermal ellipsoids for C and O at 50 % probability level, showing the same conformations. C: grey, O: red, H: white.

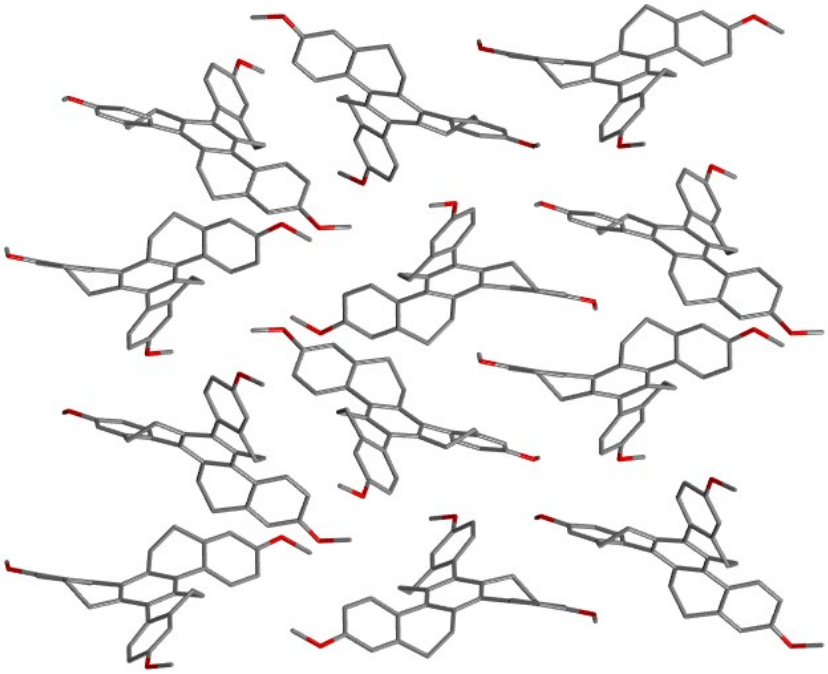

Figure S2. Stick representation of the packing along the (ac) plane. C: grey, O: red. Hydrogen atoms are omitted for clarity.

1.2 Photophysical measurements

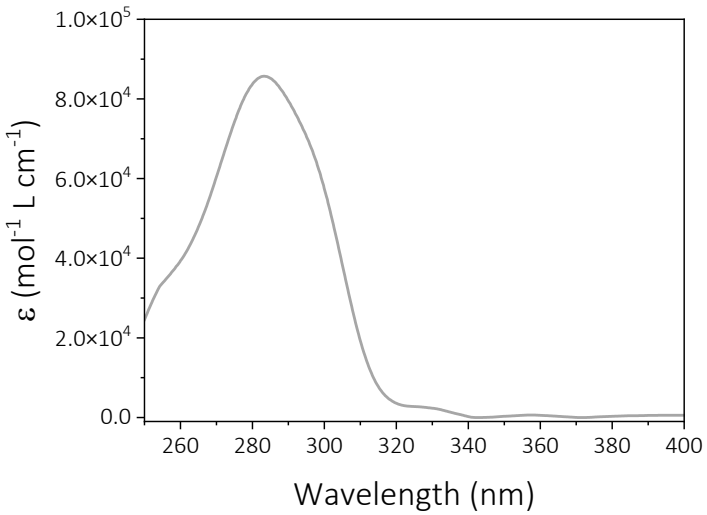

Figure S3. Absorption of **HTX-MeO** in dilute chloroform solution (10^{-5} mol L^{-1}).

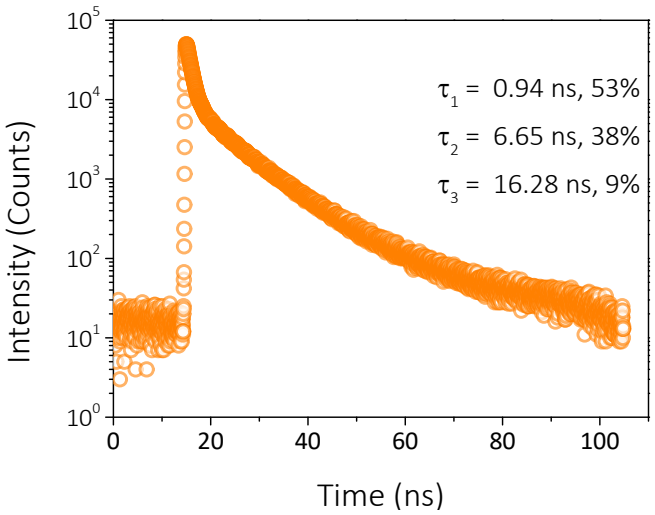

Figure S4. Time-correlated single-photon counting emission decay curves of **HTX-MeO** in 10^{-3} mol/L^{-1} 2-MeTHF solution, collected at 420 nm with excitation at 405 nm.

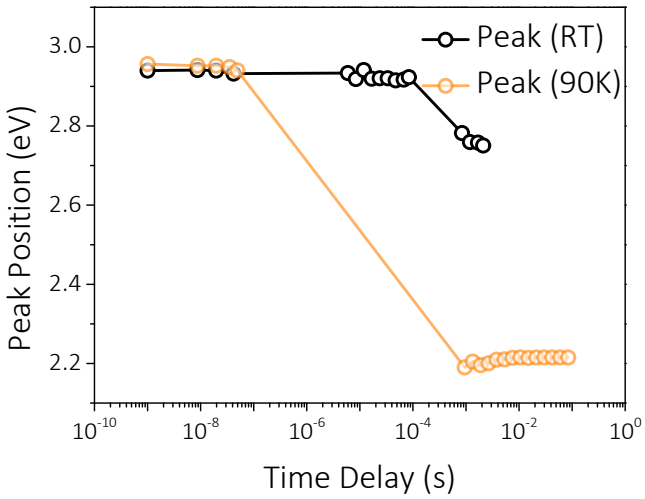

Figure S5. Shift of the emission maximum from **HTX-MeO** in 10^{-3} mol/L^{-1} 2-MeTHF solution at RT and 90 K.

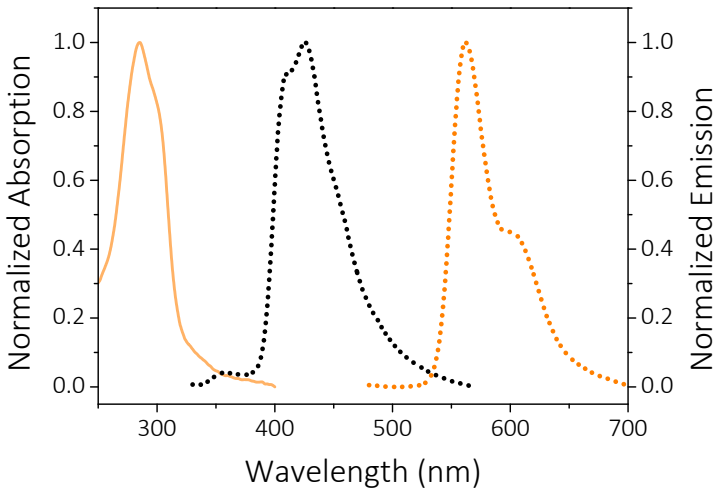

Figure S6. Normalized absorption (orange line) and emission spectra (dotted black and light orange line) in undissolved powder of **HTX-MeO** at RT with excitation at 350 nm. The Ph was obtained 10 ms after switching off the excitation at 80 K.

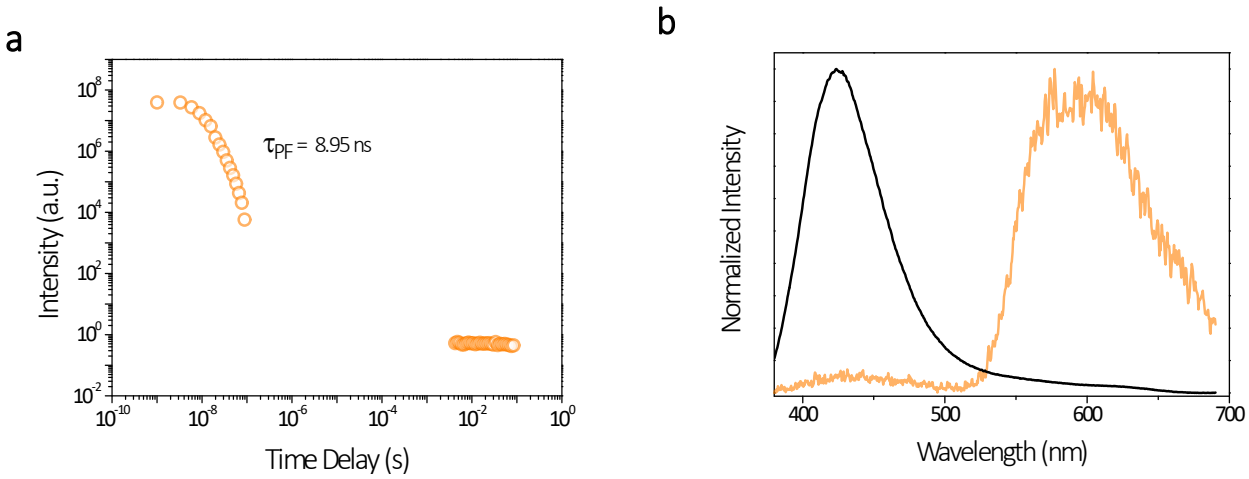

Figure S7. Time-resolved measurements of **HTX-MeO** in the powder at RT with excitation at 405 nm. (a) Time-resolved decay. (b) Normalized spectra taken at different TD: TD = 1.1 – 88.3 ns (black line); TD = 4.2 – 84.3 ms (light orange line).

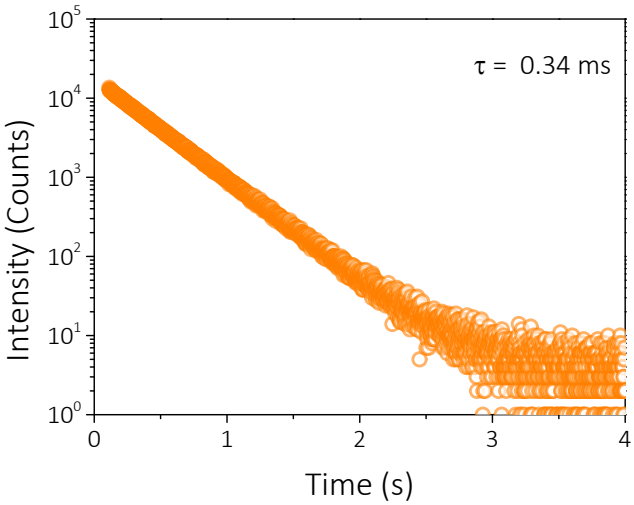

Figure S8. Time-correlated single-photon counting emission decay curves of **HTX-MeO** in powder, collected at 570 nm with excitation at 405 nm.

Table S1. Photophysical data in 2-MeTHF dilute solution and powder.

		HTX[1]	**HTX-F**[1]	**HTX-MeO**
Solution	τ_{PF} (ns) [a]	8.19	2.60	9.15
	Φ_{PF}	0.211	0.328	0.332
	τ_{Ph} (ms) [b]	498	766	245
	k_{PF} ×10^7 (s^{-1}) [c]	2.58	12.61	3.62
	k_{ISC} ×10^8 (s^{-1}) [d]	0.96	2.58	7.30
	k_{Ph} (s^{-1}) [e]	2.01	1.30	4.08
Powder	τ_{PF} (ns) [f]	11.40	8.90	8.95
	Φ_{PF}	0.410	0.197	0.434
	τ_{Ph} (ms) [b]	210	200	390
	Φ_{Ph}	0.062	0.033	0.047
	k_{PF} ×10^7 (s^{-1}) [c]	3.60	2.21	4.89
	k_{ISC} ×10^7 (s^{-1}) [d]	5.18	9.02	6.32
	k_{Ph} (s^{-1}) [g]	0.29	0.17	0.12

[a] Obtained from TCSPC measurements at RT and defined as $\tau = \Sigma \tau_i^2 A_i / \Sigma \tau_i A_i$, for a tri-exponential profile. [b] Obtained from time-resolved measurements at 90 K. [c] $k_{PF} = \Phi_{PF} / \tau_{PF}$. [d] $k_{ISC} = \Phi_{ISC} / \tau_{PF}$, considering $\Phi_{ISC} = 1 - \Phi_{PF}$ and assuming, as usual, that the Φ for internal conversion is nil, $\Phi_{IC} = 0$. [e] $k_{Ph} \sim \tau_{Ph}^{-1}$. [f] Obtained from time-resolved measurements at RT. [g] $k_{Ph} = \Phi_{Ph} / \tau_{Ph}$. The error of Φ was ±0.004.

1.3 Theoretical modeling

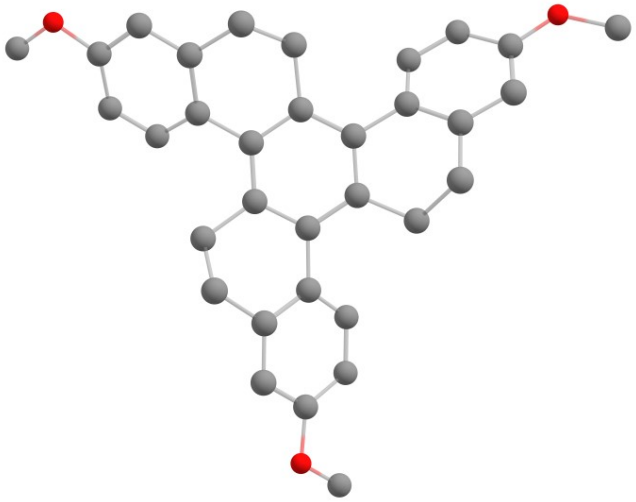

Figure S9. Optimized ground state geometry within ZORA-PBE0/def2-TZVP(-f) level of theory. The DFT ground state geometry was compared to the X-ray structure and the maximum average error found was of the order of 1.26% for bond lengths and of 0.24% for bond angles.

Table S2. Data for the TD-DFT and SOC-TD-DFT excitations within ZORA-PBE0/def2-TZVP(-f) level of theory for **HTX-MeO** in 2-MeTHF.

State	Energy		*f*	Configuration[a]
	eV	nm		
S_1	4.002	310	0.00026	H → L (31) H → L+1 (18) H-1 → L (18) H-1 → L+1 (29)
S_2	4.417	281	0.67511	H → L (54) H → L+1 (25) H-1 → L+1 (13)
S_3	4.434	280	0.80148	H → L+1 (12) H-1 → L (71)
S_4	4.448	279	0.50231	H-1 → L+1 (81) H → L+1 (38)
S_5	4.706	254	0.10855	H-2 → L+1 (28) H → L+2 (40)
T_1	3.098	400	$>1\times10^{-9}$	H → L (16) H → L+1 (26)

				H-1 → L (26) H-1 → L+1 (16)
T_2	3.457	359	1.0×10^{-9}	H → L (21) H → L+1 (16) H-1 → L (17) H-1 → L+1 (21)
T_3	3.464	358	$>1\times10^{-9}$	H → L (16) H → L+1 (21) H-1 → L (21) H-1 → L+1 (17)
T_4	3.862	321	5.0×10^{-9}	H → L (28) H → L+1 (21) H-1 → L (15) H-1 → L+1 (25)
T_5	3.926	316	1.8×10^{-8}	H-2 → L (19) H → L+3 (17)
T_6	3.963	313	1.5×10^{-8}	H-2 → L (10) H-2 → L+1 (22) H-1 → L+5 (11)
T_7	4.023	308	7.0×10^{-9}	H-2 → L+4 (15) H → L+2 (35)
T_8	4.072	305	5.3×10^{-9}	H-2 → L+4 (16) H-1 → L+2 (21) H-1 → L+4 (13)
T_9	4.088	303	3.3×10^{-9}	H-2 → L+2 (20) H-1 → L+4 (24) H → L+3 (14) H → L+5 (11)

[a] Transitions with high percentage contributions are shown in parenthesis.

References

1 G. Farias, C. A. M. Salla, M. Aydemir, L. Sturm, P. Dechambenoit, F. Durola, B. de Souza, H. Bock, A. P. Monkman and I. H. Bechtold, *Chem. Sci.*, 2021, **12**, 15116–15127.